



Urchin-Like $\text{Ni}_{2/3}\text{Co}_{1/3}(\text{CO}_3)_{1/2}(\text{OH})\cdot 0.11\text{H}_2\text{O}$ for High-Performance Supercapacitors

Zi-Min Jiang, Ting-Ting Xu*, Cong-Cong Yan, Cai-Yun Ma and Shu-Ge Dai*

Key Laboratory of Material Physics of Ministry of Education, Zhengzhou University, Zhengzhou, China

Here, we report our finding in the fabrication of novel porous urchin-like $\text{Ni}_{2/3}\text{Co}_{1/3}(\text{CO}_3)_{1/2}(\text{OH})\cdot 0.11\text{H}_2\text{O}$ (denoted as NC) nanomaterial composed of numerous nanoneedles through an one-step hydrothermal method, which delivers a high specific capacity of 318 C g^{-1} at a current density of 1 A g^{-1} . Moreover, an architectural composite electrode consisting of the porous NC nanoneedles wrapped by reduced graphene oxide (rGO) nanosheets exhibits large specific capacity (431 C g^{-1} at 1 A g^{-1}), high rate capability and long cycling life (94% capacity retention after 5,000 cycles at 20 A g^{-1}). The presence of rGO in the composite electrode greatly improves the electronic conductivity, providing efficient current collection for fast energy storage.

Keywords: porous, NiCo hydroxides, graphene, composites, supercapacitors

OPEN ACCESS

Edited by:

Qiaobao Zhang,
Xiamen University, China

Reviewed by:

Linfeng Hu,
Fudan University, China
Hongwei Mi,
Shenzhen University, China

*Correspondence:

Ting-Ting Xu
xutt@zzu.edu.cn
Shu-Ge Dai
shugedai@zzu.edu.cn

Specialty section:

This article was submitted to
Nanoscience,
a section of the journal
Frontiers in Chemistry

Received: 30 July 2018

Accepted: 31 August 2018

Published: 28 September 2018

Citation:

Jiang Z-M, Xu T-T, Yan C-C, Ma C-Y
and Dai S-G (2018) Urchin-Like
 $\text{Ni}_{2/3}\text{Co}_{1/3}(\text{CO}_3)_{1/2}(\text{OH})\cdot 0.11\text{H}_2\text{O}$
for High-Performance
Supercapacitors. *Front. Chem.* 6:431.
doi: 10.3389/fchem.2018.00431

INTRODUCTION

Supercapacitors (SCs), as an electrochemical energy storage device with high power density, long cycle life and fast charging capability, are considered as one of the most promising energy storage devices (Liang et al., 2017). The most attractive feature of SCs is its fast charging capability with large current density than other energy storage devices (Aricò et al., 2005). The structures and properties of the electrode materials are critical to the performance of the energy storage devices (Shi et al., 2017). Therefore, it has greatly attracted the interest of the researches to develop new electrode materials with excellent specific capacitance and good cycle life (Zhang et al., 2018a; Zhao et al., 2018a).

The rate performance and cycle life of the electrode materials are playing a significant role in the practicality for supercapacitors (Dai et al., 2017). Transition metal compounds such as cobalt hydroxides (Jiang et al., 2018; Long et al., 2018; Yang et al., 2018a), nickel hydroxides (Zhang et al., 2010; Ji et al., 2013; Jiang et al., 2017) with high theoretical capacity have been considered as the most promising positive electrodes for high-performance SCs. Unfortunately, the drawbacks of transition metal materials, such as limited useful cycle life and the poor rate performance, still need further improvement. One of the solutions is to design a nanostructure with large specific surface area, which can enlarge the electrode-electrolyte contact area and improve the effective utilization of the electrode materials, thereby expanding the specific capacitance of the SCs (Liu et al., 2017). Although some novel nanostructures of transition metal compounds have been reported for SCs, such as nanoparticles (Wei et al., 2014), nanowires (Zhao et al., 2018b), nanoflakes (Cao et al., 2007; Pan et al., 2018). However, the rate performance and cycle life of those electrode materials are not satisfactory, the depth of the electrode reaction decreases with the increasing current. In particular, urchin-like nanostructure composed of numerous nanounits have attracted great interest as an unusual group with well-defined nanoneedles structure and shell structure in functional materials

(Jin et al., 2018). Their unique structure possess larger surface area and higher pore volume, which are favorable for bringing about more active reaction sites in the electrolyte, the ultra-fine nano-needle structure can also effectively reduce the structural force during charging and discharging, and the electrode material has higher stability and safety.

Recently, some research results show that the composites of nickel and cobalt bimetallic electrode materials show a better cycle stability than the corresponding nickel or cobalt electrode materials because of their complementary advantages and synergistic effects (Chen et al., 2018a; Liu et al., 2018). Nonetheless, how to synthesize such electrode materials with urchin-like nanostructure in a simple and efficient way is still a challenge. In this work, we report our findings in the synthesis and characterization of the unique urchin-like nanostructure with large surface-to-volume ratio. In particular, the NC Co-doping crystal with $\text{Co}(\text{CO}_3)_x(\text{OH})_y$ anions possessed one-dimensional chain-like crystal structure was successfully prepared, which delivered a specific capacity of 318 C g^{-1} at a current density of 1 A g^{-1} . Moreover, we successfully prepared the NC/rGO nanocomposite by introducing rGO, which exhibited enhanced electrochemical performance compared to that of the NC nanomaterial.

EXPERIMENTAL SECTION

Preparation of NC Nanomaterial

All chemical reagents in this work were used as received without further purification. The urchin-like NC nanomaterial was synthesized by one-step hydrothermal method. First, 1 mmol of $\text{NiCl}_2 \cdot 6\text{H}_2\text{O}$ (aladdin, 99%), 3 mmol of $\text{CH}_4\text{N}_2\text{O}$ (aladdin, 99%) and 0.5 mol of $\text{CoCl}_2 \cdot 6\text{H}_2\text{O}$ were first dissolved in 10 mL of deionized water in the Teflon containers by stirring for 30 min to form homogeneous solution. Then the autoclave was sealed and maintained at a temperature of 100°C for 12 h. After natural cooling to room temperature, the samples were taken out, rinsed with deionized water until pH is close to 7, and dried under vacuum at 70°C overnight.

Preparation of NC/rGO Nanomaterials

The NC/rGO composite was synthesized using a hydrothermal method similar to the synthesis of NC. 1 mmol of $\text{NiCl}_2 \cdot 6\text{H}_2\text{O}$ (aladdin, 99%), 3 mmol of $\text{CH}_4\text{N}_2\text{O}$ (aladdin, 99%) and 0.5 mmol of $\text{CoCl}_2 \cdot 6\text{H}_2\text{O}$ were first dissolved in 10 mL of GO solution (2 mg mL^{-1}) in the Teflon container by stirring 30 min to form homogeneous solution. Then the autoclave was sealed and maintained at a temperature of 100°C for 12 h. After natural cooling to room temperature, the samples were taken out, rinsed with deionized water until pH is close to 7, and dried under vacuum at 70°C overnight.

Material Characterization

The phase structures of the samples were characterized by X-ray diffraction (XRD) analysis (XRD, PA National X' Pert Pro with $\text{Cu K}\alpha$ radiation), The microstructure and morphology

of NC nanomaterials were characterized using field emission scanning electron microscopy (Zeiss, sigma300) and high-resolution transmission electron microscopy (HRTEM, JEOL, JEM-2100) with energy dispersive X-ray spectrometry (EDS). The nitrogen adsorption-desorption isotherm measurement of the sample was performed using a ASAP2420-4MP. The specific surface area was obtained by the Brunauer-Emmett-Teller (BET) method. The element atomic ratio analysis were characterized by inductively coupled plasma mass spectrometry (ICP MS) using a Agilent 7700.

Electrochemical Measurement

The as-prepared NC and NC/rGO electrodes were used as the working electrodes with a platinum sheet electrode and a Ag/AgCl (prefilled with 4M KCl aqueous solution saturated with AgCl) reference electrodes (Gogotsi, 2014), respectively. The electrochemical tests were performed using a CHI760 electrochemical workstation. Cyclic voltammetry (CV), galvanostatic charge-discharge (GCD) and electrochemical impedance spectroscopy (EIS) tests were carried out using a three-electrode configuration in 2M KOH aqueous solution at room temperature. For the working electrode, a mixture containing of 80 wt% electroactive material, 10 wt% Super P Li (TIMCAL Graphite and Carbon) powders, and 10 wt% polytetrafluoroethylene (PTFE) binder was well mixed to prepare working electrodes, and then rolled with the assistance of ethanol to form a uniform film with a typical area mass loading of approximately 1.5 mg cm^{-2} , and dried under vacuum at 80°C for 12 h, then pressed it between two nickel foams. The cyclic voltammograms were acquired in a potential range of 0–0.5 V at different scan rates, the charge-discharge processes were performed by cycling the potential from 0 to 0.45 V at different current densities in a 2M KOH aqueous electrolyte, and the EIS was performed in the frequency range from 0.01 Hz to 100 k Hz under open-circuit condition. The specific capacity Q

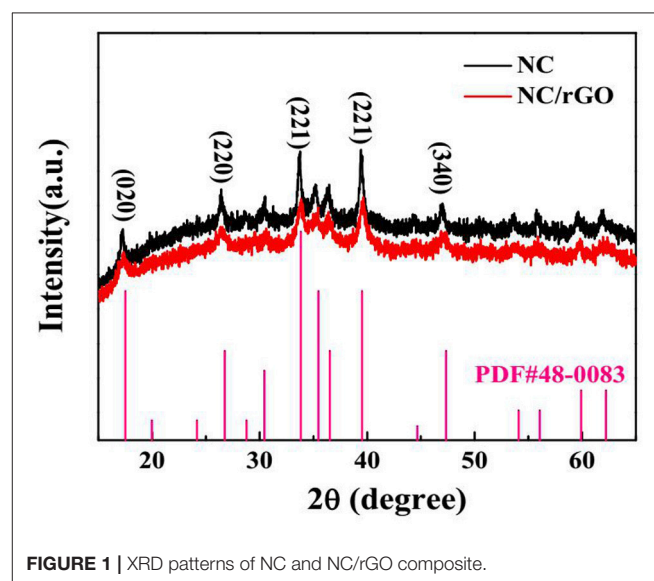


FIGURE 1 | XRD patterns of NC and NC/rGO composite.

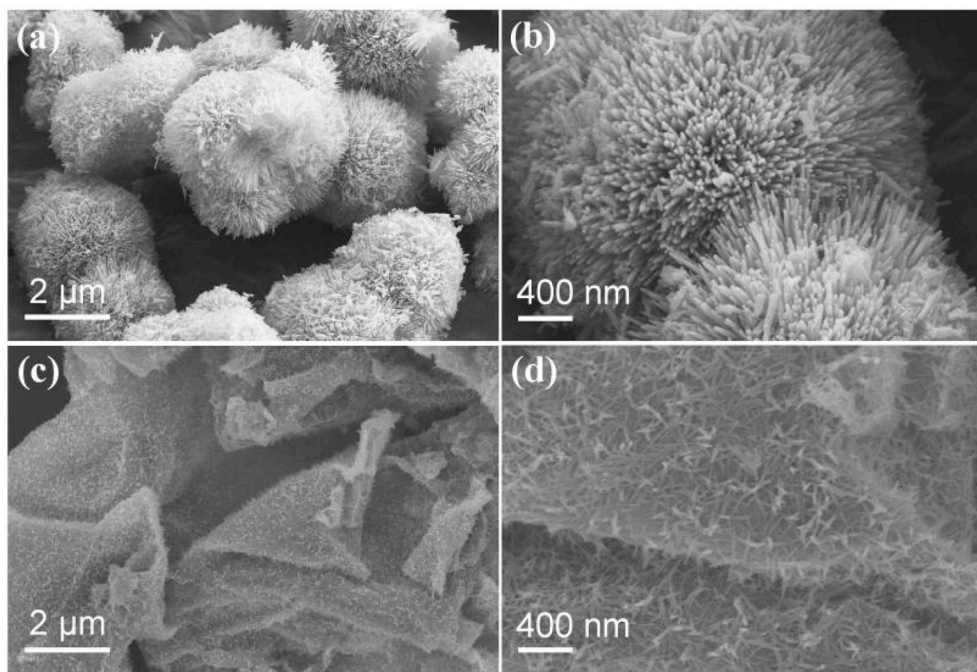


FIGURE 2 | Scanning electron microscopy (SEM) images of as-synthesized NC and NC/rGO nanomaterials. **(a,b)** urchin-like NC nanoball, **(c,d)** as-synthesized NC/rGO composite nanosheets.

($C\ g^{-1}$) of the battery-type electrodes was calculated as follows (Mai et al., 2013):

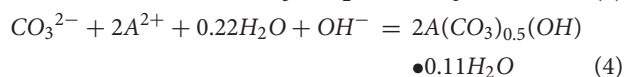
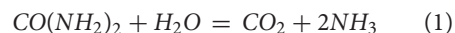
$$Q = i_m \Delta t \quad (1)$$

where $i_m = I/m$ ($A\ g^{-1}$) is the current density, I is the current, m is the mass of the active electrode material and Δt is the discharge time.

RESULTS AND DISCUSSION

It is well known that the polymorphs of nickel hydroxides depend on the hydrothermal reaction conditions such as the ratio of precursors, reaction temperature and time (Li et al., 2016). By tuning the initial mole ratio of reactants, we synthesized the urchin-like NC nanomaterials by a simple one-step solvent-thermal method. The XRD pattern of the NC (black curve) sample is illustrated in **Figure 1**. All diffraction peaks of the XRD pattern can be indexed to orthorhombic $Co(CO_3)_{1/2}(OH) \cdot 0.11H_2O$ (JCPDS NO. 48-0083). The strong diffraction peaks centered at $2\theta = 17.2^\circ, 26.4^\circ, 33.8^\circ, 39.4^\circ,$ and 46.9° , attributed to $(0\ 2\ 0), (2\ 2\ 0), (2\ 2\ 1), (2\ 3\ 1),$ and $(3\ 4\ 0)$, respectively. And the XRD pattern of NC/rGO (red curve) sample is extremely similar to the NC pattern, and no other obvious peaks are detected. The reaction mechanism may be as follows

(Wei et al., 2017):



In the chemical reaction system, firstly, $CO(NH_2)_2$ combined with H_2O to produce CO_2 and NH_3 (equation 1). Then, CO_2 and NH_3 combined with H_2O immediately to produce CO_3^{2-} , OH^- and NH_4^+ (equations 2 and 3), respectively. Finally, CO_3^{2-} and OH^- combined with A^{2+} (Ni^{2+} or Co^{2+}) to form the sample (equation 4).

SEM was performed to examine the morphology and structure of the as-synthesized samples. **Figure 2a** shows the low-magnification SEM image of as-synthesized NC nanomaterial, which appears to be thorn balls constructed of numerous nanoneedles, and similar to the urchin-like microspheres. In **Figure 2b**, the high magnification SEM image reveals that the diameters of those nanoneedles are around 10–20 nm. The morphology evolution mechanism of urchin-like NC may be as follows: firstly, the ultrashort nanoneedles *in situ* grow on the surface of the solid core as the self-generated templet without crack and finish solid core growth. Owing to the increasing of the amount of NH_3 and CO_3^{2-} , NH_3 holds the metal ions moving to the top of the ultrashort nanoneedles with high surface energy and generates precipitate, which

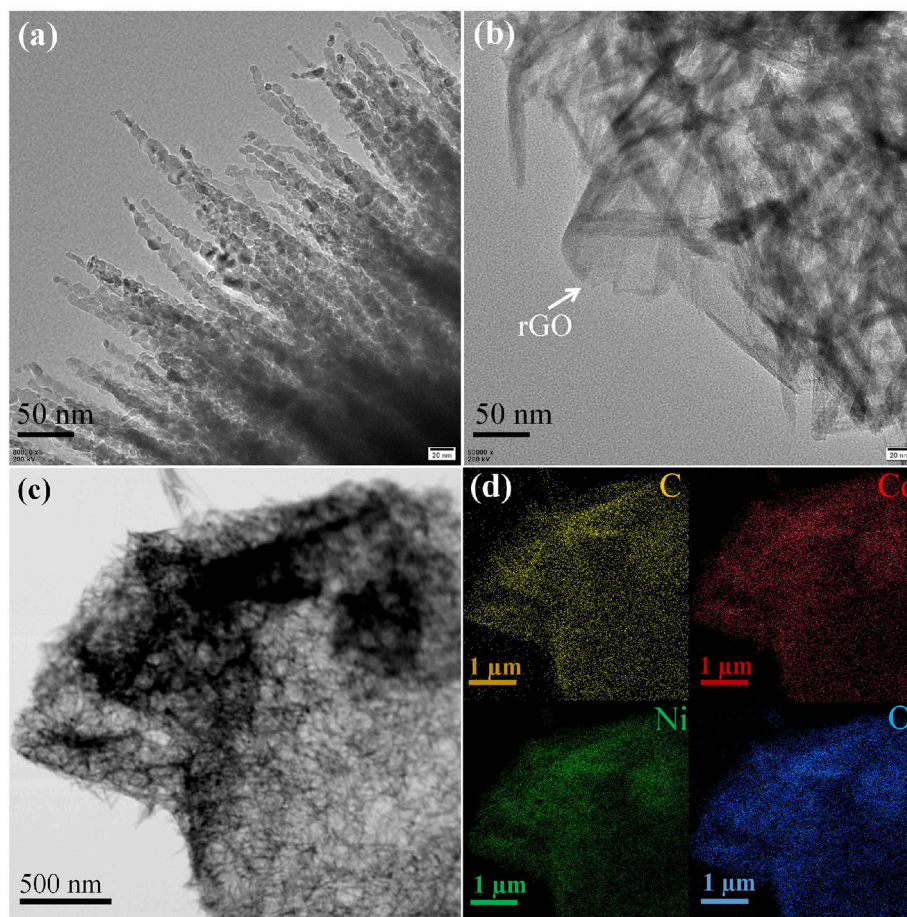


FIGURE 3 | TEM image of NC and NC/rGO composite. **(a)** high magnification of NC urchin-like nanoneedles, **(b)** high magnification of NC/rGO composite nanosheets, **(c)** the bright field TEM image of NC/rGO composite nanosheets. **(d)** TEM-EDX mapping images NC/rGO composite nanosheets.

TABLE 1 | Results of ICP-MS for NC-1 and NC-2 and NC-3.

Sample name	SOLUTION CONCENTRATION (MG L ⁻¹)		
	Ni	Co	Atomic ratio of Ni:Co
NC-1	8.3046	4.3271	69.56:36.71
NC-2	8.4231	4.3657	70.55:37.04
NC-3	8.3546	4.3520	69.98:36.92

leads to the preferred growth of product at the top of short nanoneedles and makes the short nanoneedles slowly into the long nanoneedles. The SEM images of the NC/rGO samples are shown in **Figures 2c,d**, and the morphology of the composite is nanosheets. These NC nanoneedles are distributed uniformly in the rGO nanosheets, and numerous nanosheets overlap together to form an irregular three-dimensional architecture. Notably, this unique nanostructure with large surface is favorable for efficient and fast transport of the electrolyte to the surface of the active materials, thus improving the effective utilization of the active material. The high magnification TEM images (**Figures 3a,b**) show the clear morphology of

the nanoneedles in the NC and NC/rGO materials. These nanoneedles with a diameter of 10~20 nm (**Figure 3a**) build a unique urchin-like nanostructure, which greatly shorts the electron transport channel, and improves the conductivity of the electrodes. In **Figure 3b**, the NC nanoneedles are attached to the rGO nanosheets, forming a composite nanostructure. However, the urchin-like suffered from the deficiency of those shells, the internal active material could not make full contact with the electrolyte and then affect the performance of the whole electrode. Fortunately, the addition of rGO nanosheet overcomes this shortcoming, these nanoneedles distributed uniformly on the graphene nanosheets, which provides an effective pathway for charge transport, weakens the polarization phenomenon at high current, and further improves the effective utilization of the active material and the rate performance of the electrodes. **Figures 3c,d** shows the bright field TEM image and mapping images of the NC/rGO composite, which clearly reveals that the NC nanoneedles are distributed homogeneously in the rGO nanosheets. The molar ratio of Ni:Co is determined to be 2:1 based on the result analysis, which is similar to the results of ICP-MS (~70.03:36.89, **Table 1**), and close to the mole ratio of adding nickel and cobalt

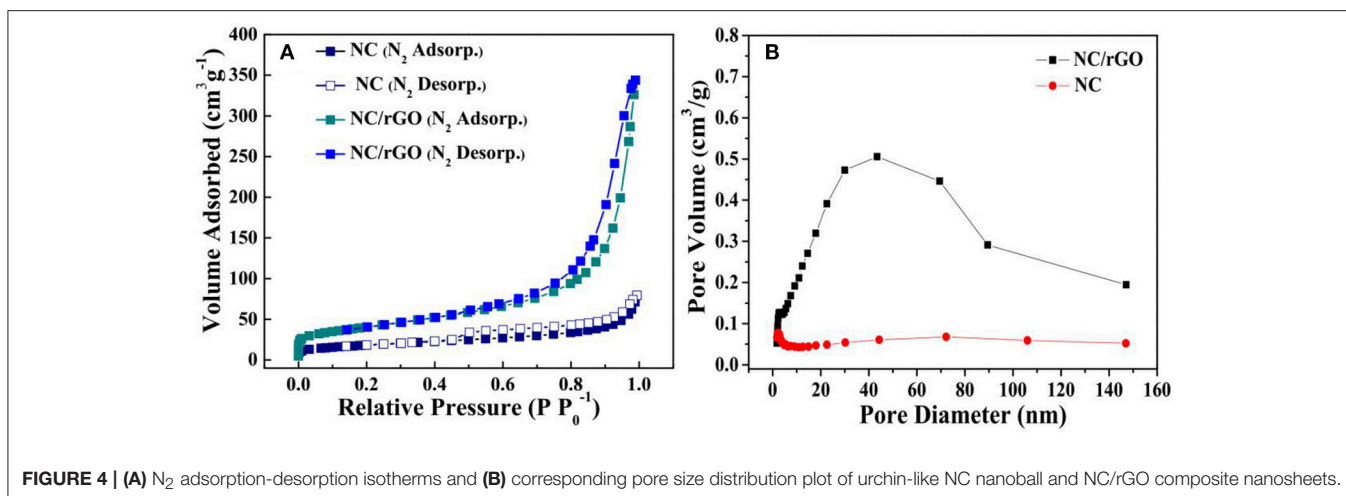


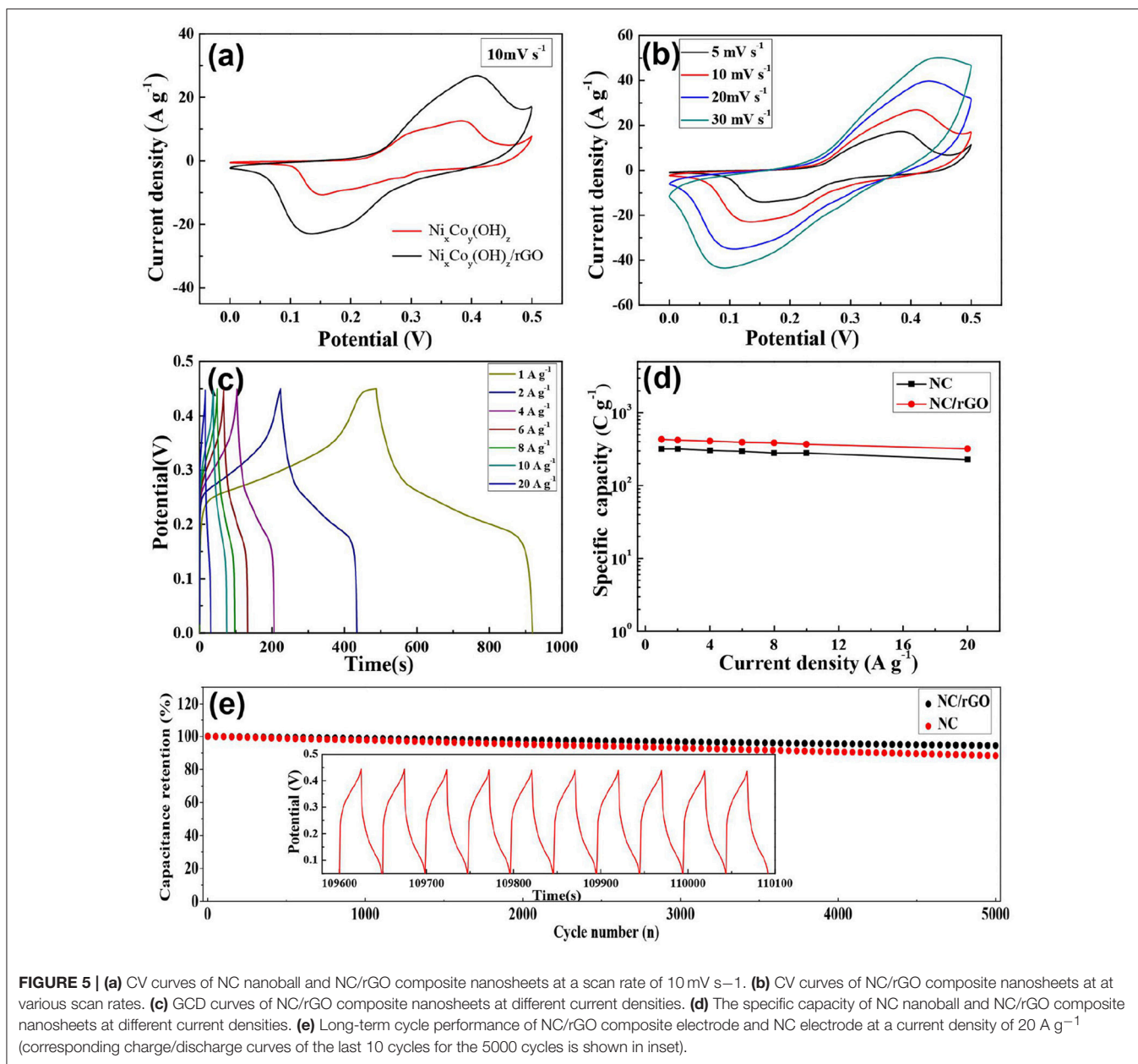
FIGURE 4 | (A) N₂ adsorption-desorption isotherms and **(B)** corresponding pore size distribution plot of urchin-like NC nanoball and NC/rGO composite nanosheets.

sources, proving that urchin-like NC nanomaterial possesses a molecular formula of NC. To investigate the porosity and surface area of as-prepared samples, N₂ adsorption-desorption isotherms of NC and NC/rGO conducted at 77.350 K were investigated and are displayed in **Figure 4A**. Through Brunauer-Emmett-Teller (BET) analysis, the surface areas of NC and NC/rGO composite were identified as 62.55 m²g⁻¹ and 138.27 m²g⁻¹, respectively. In addition, the pore size distribution curves were also investigated via using Barrett-Joyner-Halenda (BJH) method (**Figure 4B**). For NC, no obvious peaks arise in the entire range of pore size distribution curve. For NC/rGO, an obvious peak at around 40~50 nm in the pore size distribution curve was observed, which was attributed to the rGO sheets. These nanosheets provide a lot of attachment points for the growth of nanoneedles through the hydrothermal treatment. Higher surface area offers abundant reaction sites and enhances the specific capacity of the NC/rGO composite electrodes.

The electrochemical performance of the NC microspheres and NC/rGO nanocomposite were first evaluated with a three-electrode configuration in 2 M KOH aqueous electrolyte, the results are shown in **Figures 5a–d** and **Figure S1**. For comparison, the electrochemical performance of NC and NC/rGO electrodes in the potential range between 0 and 0.5 V (versus Ag/AgCl) at a scan rate of 10 mV s⁻¹ are demonstrated in **Figure 5a**. Evidently, the NC/rGO electrode exhibits a higher current density and larger increment in the CV integrated area than NC electrode, which indicates an obvious enhanced electrochemical reaction activity and charge storage, suggesting the improvement of conductivity and electrochemical performance. **Figure 5b** displays the CV curves of the NC/rGO composite electrode at different scan rates; all the CV curves exhibit a pair of redox peak, which indicates that the energy storage in our electrodes appears to be battery-type materials. The corresponding CV curves of NC microspheres was also collected and shown in **Figure S2**. It is clear that all of the plateaus at around 0.05–0.15 V, which correspond to the redox processes. Compared with the CV curves of NC, all of the CV curves of the NC/rGO composite electrode turn into smooth, indicating

that the rGO greatly improved the conductivity of the composite electrodes.

The specific capacities of the NC and NC/rGO electrodes were calculated based on the GCD curves, and the corresponding GCD curves of NC and NC/rGO electrodes are shown in **Figure S2** and **Figure 5c**, respectively. As shown in **Figure 5d**, the NC electrode delivered a specific capacity of 318 C g⁻¹ at a current density of 1 A g⁻¹, and retained ~71% (228 C g⁻¹) of the capacity when the current density was increased from 1 to 20 A g⁻¹. In comparison, the NC/rGO electrode exhibited a specific capacity of 431 C g⁻¹ at a current density of 1 A g⁻¹, and retained ~74% (320 C g⁻¹) of capacity, which is higher than that of the NC electrode. The obvious discharge platform further proves the Faraday energy storage mode, demonstrating that the composite electrodes possess battery-like effect in the charge and discharge process (Yang et al., 2018b). Besides, the specific capacity of the NC/rGO were higher than other transition metal compounds reported in literature, such as Co_{0.45}Ni_{0.55}O/RGO nanocomposites (411 C g⁻¹ at a current density of 1 A g⁻¹) (Xiao and Yang, 2012), NiCo₂-RGO nanocomposites (417 C g⁻¹ at a current density of 1 A g⁻¹) (Wang et al., 2011), NiCo₂O₄ nanocomposites (296 F g⁻¹ at a current density of 1 A g⁻¹) (Xiao and Yang, 2011). The good electrochemical performance of NC/rGO composite nanomaterial may be attributed to its unique morphology and crystal structure. First, the self-contained OH⁻ and the one-dimensional chain-like crystal structure unit increase the electrode material ionic conductivity. Second, the porous composite nanostructure has large specific surface area of 138.27 m²g⁻¹, which greatly increases the effective area between active material and electrolyte, and facilitates more effective exposure of surface active sites for fast Faradic redox reaction. Third, the rGO nanosheets provides a great specific area for the NC nanoneedles growth, constructing a three-dimensional conducting network, which ensures the excellent rate performance. Cycling life is an important property for the SCs. The NC/rGO composite electrode could still retain ~94% of the initial capacity over 5,000 cycles at a high current density of 20 A g⁻¹, which is higher than the NC electrode



(~88% of the initial capacity), revealing its good cycling stability (Figure 5e). Furthermore, the cycling stability of the NC/rGO in 2 M aqueous KOH aqueous solution using a typical three-electrode cell were superior to many transition metal compounds electrode materials reported in literature, such as Co(OH)₂ nanosheets (89.1% capacitance retention after 5,000 cycles at 20 A g⁻¹) (Chen et al., 2018b), Co-doped α -Ni(OH)₂/RGO nanosheet (87.9% capacitance retention after 1,000 cycles at 10 A g⁻¹) (Zhang et al., 2018b), Ni(OAc)₂/Co(NO₃)₂ (91.5% capacitance retention after 1,000 cycles at 5 A g⁻¹) (Wei et al., 2018), illustrating the excellent capacity and long-term electrochemical stability of the NC/rGO composite electrode.

CONCLUSION

In summary, a novel porous NC nanomaterial with urchin-like architecture has been successfully prepared by one-step hydrothermal process. When tested in a three-electrode configuration in 2 M KOH aqueous electrolyte, it is found that the NC nanomaterial exhibits a high specific capacity of 318 C g⁻¹ at 1 A g⁻¹. Moreover, a porous NC/rGO composite electrode was also successfully prepared, which exhibited good specific capacity (431 C g⁻¹ at 1 A g⁻¹), great rate capability (~74% capacity retention) and long cycling life (94% capacity retention over 5,000 cycles), demonstrating its promising potential for the high-performance supercapacitors.

AUTHOR CONTRIBUTIONS

Z-MJ carried out the material preparation and electrochemical test; T-TX and S-GD carried out and analyzed the XRD, SEM, and TEM analysis; Z-MJ wrote the paper and all authors discussed the results; Z-MJ, T-TX, C-CY, C-YM and S-GD revised the manuscript; T-TX attained the main financial support for the research and supervised all the experiments.

ACKNOWLEDGMENTS

This work was supported by the National Natural Science Foundation of China (Grant No. 11504331), the China Postdoctoral Science Foundation (Grant No. 2015M582196,

Grant No. 2015M582193, Grant No. 2015M582194, Grant No. 2018M630831), the Outstanding Young Talent Research Fund of Zhengzhou University (Grant No. 1521317005, Grant No. 1521317001), the National Natural Science Foundation of China (Grant No. 21805247), the National Natural Science Foundation of China (Grant No. 21805247), the China Postdoctoral Science Foundation (Grant No. 2018M630831).

SUPPLEMENTARY MATERIAL

The Supplementary Material for this article can be found online at: <https://www.frontiersin.org/articles/10.3389/fchem.2018.00431/full#supplementary-material>

REFERENCES

- Aricò, A. S., Bruce, P., Scrosati, B., Tarascon, J. M., and Van Schalkwijk, W. (2005). Nanostructured materials for advanced energy conversion and storage devices. *Nat. Mater.* 4, 366–377. doi: 10.1038/nmat1368
- Cao, M., He, X., Chen, J., and Hu, C. (2007). Self-assembled nickel hydroxide three-dimensional nanostructures: a nanomaterial for alkaline rechargeable batteries. *Cryst. Growth Des.* 7, 170–174. doi: 10.1021/cg060524w
- Chen, F., Wang, H., Ji, S., Linkov, V., and Wang, R. (2018a). Core-shell structured Ni₃S₂@Co(OH)₂ nano-wires grown on Ni foam as binder-free electrode for asymmetric supercapacitors. *Chem. Eng. J.* 345, 48–57. doi: 10.1016/j.cej.2018.03.152
- Chen, M., Qu, G., Yang, W., Li, W., and Tang, Y. (2018b). Celgard membrane-mediated ion diffusion for synthesizing hierarchical Co(OH)₂ nanostructures for electrochemical applications. *Chem. Eng. J.* 350, 209–216. doi: 10.1016/j.cej.2018.05.183
- Dai, S., Zhao, B., Qu, C., Chen, D., Dang, D., Song, B., et al. (2017). Controlled synthesis of three-phase Ni_xS_y/rGO nanoflake electrodes for hybrid supercapacitors with high energy and power density. *Nano Energy* 33, 522–531. doi: 10.1016/j.nanoen.2017.01.056
- Gogotsi, Y. (2014). What nano can do for energy storage. *ACS Nano* 8, 5369–5371. doi: 10.1021/nn503164x
- Ji, J., Zhang, L. L., Ji, H., Li, Y., Zhao, X., Bai, X., et al. (2013). Nanoporous Ni(OH)₂ thin film on 3D Ultrathin-Graphite foam for asymmetric supercapacitor. *ACS Nano* 7, 6237–6243. doi: 10.1021/nn4021955
- Jiang, Y., Song, Y., Li, Y., Tian, W., Pan, Z., Yang, P., et al. (2017). Charge transfer in ultrafine LDH Nanosheets/Graphene interface with superior capacitive energy storage performance. *ACS Appl. Mater. Inter.* 9, 37645–37654. doi: 10.1021/acsami.7b09373
- Jiang, Y., Wu, Z., Jiang, L., Pan, Z., Yang, P., Tian, W., et al. (2018). Freestanding CoSeO₃.H₂O nanoribbon/carbon nanotube composite paper for 2.4 V high-voltage, flexible, solid-state supercapacitors. *Nanoscale* 10, 12003–12010. doi: 10.1039/C8NR02924E
- Jin, Y., Zhao, C., Jiang, Q., and Ji, C. (2018). Preparation and electrochemical capacitive performance of hollow urchin-like Ni₂P/CoP bimetallic phosphides for high-performance supercapacitors. *Mater. Lett.* 219, 59–63. doi: 10.1016/j.matlet.2018.02.068
- Li, W., Wang, S., Xin, L., Wu, M., and Lou, X. (2016). Single-crystal β-NiS nanorod arrays with a hollow-structured Ni₃S₂ framework for supercapacitor applications. *J. Mater. Chem. A* 4, 7700–7709. doi: 10.1039/C6TA01133K
- Liang, H., Xia, C., Jiang, Q., Gandi, A. N., Schwingenschlögl, U., and Alshareef, H. N. (2017). Low temperature synthesis of ternary metal phosphides using plasma for asymmetric supercapacitors. *Nano Energy* 35, 331–340. doi: 10.1016/j.nanoen.2017.04.007
- Liu, S., Zeng, Y., Zhang, M., Xie, S., Tong, Y., Cheng, F., et al. (2017). Binder-free WS₂ nanosheets with enhanced crystallinity as a stable negative electrode for flexible asymmetric supercapacitors. *J. Mater. Chem. A* 5, 21460–21466. doi: 10.1039/C7TA07009H
- Liu, Y., Lu, Q., Huang, Z., Sun, S., Yu, B., Evariste, U., et al. (2018). Electrodeposition of Ni-Co-S nanosheet arrays on N-doped porous carbon nanofibers for flexible asymmetric supercapacitors. *J. Alloy. Compd.* 762, 301–311. doi: 10.1016/j.jallcom.2018.05.239
- Long, J. Y., Yan, Z. S., Gong, Y., and Lin, J. H. (2018). MOF-derived Cl/O-doped C/CoO and C nanoparticles for high performance supercapacitor. *Appl. Surf. Sci.* 448, 50–63. doi: 10.1016/j.apsusc.2018.04.068
- Mai, L., Minhas-Khan, A., Tian, X., Hercule, K. M., Zhao, Y., Lin, X., et al. (2013). Synergistic interaction between redox-active electrolyte and binder-free functionalized carbon for ultrahigh supercapacitor performance. *Nat. Commun.* 4:2923. doi: 10.1038/ncomms3923
- Pan, Z., Jiang, Y., Yang, P., Wu, Z., Tian, W., Liu, L., et al. (2018). *In situ* growth of layered bimetallic ZnCo hydroxide nanosheets for high-performance all-solid-state pseudocapacitor. *ACS Nano* 12, 2968–2979. doi: 10.1021/acsnano.8b00653
- Shi, P., Li, L., Hua, L., Qian, Q., Wang, P., Zhou, J., et al. (2017). Design of amorphous manganese oxide@multiwalled carbon nanotube fiber for robust solid-state supercapacitor. *ACS Nano* 11, 444–452. doi: 10.1021/acsnano.6b06357
- Wang, H., Hu, Z., Chang, Y., Chen, Y., Wu, H., Zhang, Z., et al. (2011). Design and synthesis of NiCo₂O₄-reduced graphene oxide composites for high performance supercapacitors. *J. Mater. Chem.* 21, 10504–10511. doi: 10.1039/c1jm10758e
- Wei, M., Huang, Q., Zhou, Y., Peng, Z., and Chu, W. (2018). Ultrathin nanosheets of cobalt-nickel hydroxides hetero-structure via electrodeposition and precursor adjustment with excellent performance for supercapacitor. *J. Energy Chem.* 27, 591–599. doi: 10.1016/j.jechem.2017.10.022
- Wei, W., Cui, S., Ding, L., Mi, L., Chen, W., and Hu, X. (2017). Urchin-Like Ni_{1/3}Co_{2/3}(CO₃)_{1/2}(OH)·0.11H₂O for ultrahigh-rate electrochemical supercapacitors: structural evolution from solid to hollow. *ACS Appl. Mater. Inter.* 9, 40655–40670. doi: 10.1021/acsami.7b12392
- Wei, W., Mi, L., Gao, Y., Zheng, Z., Chen, W., and Guan, X. (2014). Partial ion-exchange of nickel-sulfide-derived electrodes for high performance supercapacitors. *Chem. Mater.* 26, 3418–3426. doi: 10.1021/cm5006482
- Xiao, J., and Yang, S. (2011). Sequential crystallization of sea urchin-like bimetallic (Ni, Co) carbonate hydroxide and its morphology conserved conversion to porous. *RSC Adv.* 1, 588–595. doi: 10.1039/C1RA00342A
- Xiao, J., and Yang, S. (2012). Bio-inspired synthesis of NaCl-type CoxNi1-xO (0 ≤ x < 1) nanorods on reduced graphene oxide sheets and screening for asymmetric electrochemical capacitors. *J. Mater. Chem.* 22, 12253–12262. doi: 10.1039/c2jm31057k
- Yang, P., Wu, Z., Jiang, Y., Pan, Z., Tian, W., Jiang, L., et al. (2018b). Fractal(Nix Co1-x)9Se8 nanodendrite arrays with highly exposed(011) surface for wearable, all-solid-statesupercapacitor. *Adv. Energy Mater.* 8, 1801392. doi: 10.1002/aenm.201801392
- Yang, W., Qu, G., Chen, M., Ma, W., Li, W., and Tang, Y. (2018a). Effective NaBH₄-exfoliated ultrathin multilayer Co(OH)₂ nanosheets arrays and sulfidation for energy storage. *Nanotechnology* 29:295403. doi: 10.1088/1361-6528/aac158

- Zhang, L., Song, S., and Shi, H. (2018b). One-pot methanol-mediated solvothermal synthesis of 3D porous Co-doped α -Ni(OH)₂/RGO nanosheets as a high-performance pseudo-capacitance electrode. *J. Alloy. Compd.* 751, 69–79. doi: 10.1016/j.jallcom.2018.04.109
- Zhang, Q., Liu, Z., Zhao, B., Cheng, Y., Zhang, L., Wu, H., et al. (2018a). Design and understanding of dendritic mixed-metal hydroxide nanosheets@N-doped carbon nanotube array electrode for high-performance asymmetric supercapacitors. *Energy Storage Materials* doi: 10.1016/j.ensm.2018.06.026
- Zhang, X., Shi, W., Zhu, J., Zhao, W., Ma, J., Mhaisalkar, S., et al. (2010). Synthesis of porous NiO nanocrystals with controllable surface area and their application as supercapacitor electrodes. *Nano Res.* 3, 643–652. doi: 10.1007/s12274-010-0024-6
- Zhao, B., Zhang, L., Zhang, Q., Chen, D., Cheng, Y., Deng, X., et al. (2018a). Rational design of nickel hydroxide-based nanocrystals on graphene for ultrafast energy storage. *Adv. Energy Mater.* 8, 1702247. doi: 10.1002/aenm.201702247
- Zhao, Y., He, X., Chen, R., Liu, Q., Liu, J., Song, D., et al. (2018b). Hierarchical NiCo₂S₄@CoMoO₄ core-shell heterostructures nanowire arrays as advanced electrodes for flexible all-solid-state asymmetric supercapacitors. *Appl. Surf. Sci.* 453, 73–82. doi: 10.1016/j.apsusc.2018.04.159

Conflict of Interest Statement: The authors declare that the research was conducted in the absence of any commercial or financial relationships that could be construed as a potential conflict of interest.

Copyright © 2018 Jiang, Xu, Yan, Ma and Dai. This is an open-access article distributed under the terms of the Creative Commons Attribution License (CC BY). The use, distribution or reproduction in other forums is permitted, provided the original author(s) and the copyright owner(s) are credited and that the original publication in this journal is cited, in accordance with accepted academic practice. No use, distribution or reproduction is permitted which does not comply with these terms.